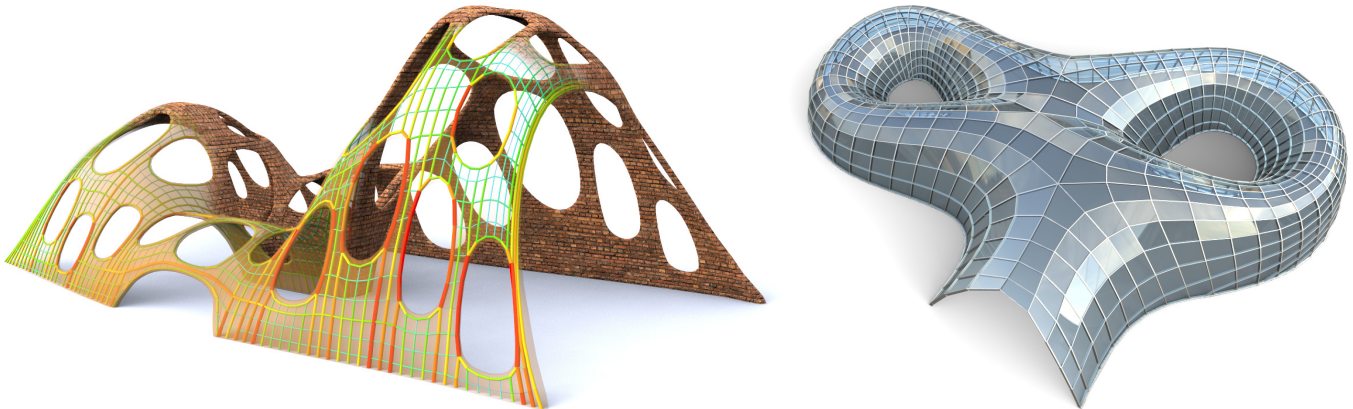


# Design of Self-supporting Surfaces



**Figure 1:** Left: *Surfaces with irregularly placed holes are hard to realize as masonry, where the mortar between bricks must not be subject to tensile stresses. The surface shown here has this surprising property – it has been found as the nearest self-supporting shape from a given freeform geometry. The fictitious thrust network used in our algorithms is also shown, with edges' cross-section and coloring visualizing the magnitude of forces (warmer colors represent higher stresses.)* Right: *Curvature analysis with respect the so-called Airy stress surface tells us how to remesh shapes by self-supporting quad meshes with planar faces, which guide steel/glass constructions with low moments in nodes.*

## 1 Abstract

Self-supporting masonry is one of the most ancient and elegant techniques for building curved shapes. Because of the very geometric nature of their failure, analyzing and modeling such structures is more a geometry processing problem than one of classical continuum mechanics. In this paper we use the thrust network method of analysis and present an iterative nonlinear optimization algorithm for efficiently approximating freeform shapes by self-supporting ones. The rich geometry of thrust networks leads us to close connections between different topics of discrete differential geometry, such as a finite-element discretization of the Airy stress potential, perfect graph Laplacians, and the problem of computing admissible loads via curvatures of polyhedral surfaces. This geometric viewpoint allows us, in particular, to remesh self-supporting shapes by self-supporting quad meshes with planar faces. This leads to another application of the theory: steel/glass constructions with low moments in nodes.

**CR Categories:** I.3.5 [Computer Graphics]: Computational Geometry and Object Modeling—Curve, surface, solid, and object representations;

**Keywords:** Discrete differential geometry, architectural geometry, self-supporting masonry, thrust networks, reciprocal force diagrams, discrete Laplace operators, isotropic geometry, mean curvature

## 2 Introduction

Vaulted masonry structures are among the simplest and at the same time most elegant solutions for creating curved shapes in building construction. For this reason they have been an object of interest since antiquity; large, non-convex examples of such structures include gothic cathedrals. They continue to be an active topic of research today.

Our paper is concerned with a combined geometry+statics analysis of *self-supporting* masonry and with tools for the interactive modeling of freeform self-supporting structures. Here “self-supporting” means that the structure, considered as an arrangement of blocks (bricks, stones), holds together by itself, with additional support present only during construction. This analysis is based on the following assumptions, which follow the classic [Heyman 1966]:

*Assumption 1:* Masonry has no tensile strength, but the individual building blocks do not slip against each other (because of friction or mortar). On the other hand, their compressive strength is sufficiently high so that failure of the structure is by a sudden change in geometry and not by material failure.

*Assumption 2 (The Safe Theorem):* If a system of forces can be found which is in equilibrium with the load on the structure and which is contained within the masonry envelope then the structure will carry the loads, although the actual forces present may not be those postulated by that system.

Our approach is twofold: We first give an overview of the continuous case of a smooth surface under stress, which turns out to be governed locally by the so-called Airy stress function. This mathematical model is called a membrane in the engineering literature and has been applied to the analysis of masonry before. The surface is self-supporting if and only if stresses are entirely compressive. For computational purposes, stresses are discretized as a fictitious *thrust network* [Block and Ohsendorf 2007] contained in the masonry structure; this network is a system of forces in equilibrium with the structure’s deadload. It can be interpreted as a finite element discretization of the continuous case, and it turns out to have very interesting geometry, with the Airy stress function becoming a polyhedral surface directly related to a reciprocal force diagram.

While previous work in architectural geometry was mostly concerned with aspects of rationalization and purely geometric side-conditions which occur in freeform architecture, the focus of this paper is design with *statics* constraints. In particular, our contributions are the following:

67 **Contributions.**

- 68 • We present an optimization algorithm, based on the theory of  
69 thrust networks and Airy potentials, for efficiently finding a  
70 self-supporting surface near a given arbitrary reference surface (§3), and build a tool for interactive design of self-sup-  
71 porting surfaces based on this algorithm (§4). Freeform ma-  
72 sonry is based on such surfaces.
- 73
- 74 • The discrete “stress Laplacian” derived from a thrust network  
75 with compressive forces is a so-called perfect one (§2.2). We  
76 use it to argue why our discretizations are faithful to the con-  
77 tinuous case.
- 78
- 79 • We connect the physics of self-supporting surfaces with the  
80 geometry of isotropic 3-space , and express the equations gov-  
81 erning self-supporting surfaces in terms of curvatures (§2.3)  
82 and (§2.4). Likewise we establish a connection between the  
83 stress Laplacian and mean curvatures of polyhedral surfaces.  
84 This theoretical part of the paper is a contribution to Discrete  
85 Differential Geometry.
- 86
- 87 • We use the geometric knowledge we have gathered to find par-  
88 ticularly nice families of self-supporting surfaces, especially  
89 planar quadrilateral representations of thrust networks (§5).  
This leads to steel/glass structures with low bending and tor-  
sion moments.

90 **Related Work.** Unsupported masonry has been an active topic of  
91 research in the engineering community. The foundations for the  
92 modern approach were laid by Jacques Heyman [1966] and are  
93 available as the textbook [Heyman 1995]. The theory of reciprocal  
94 force diagrams in the planar case was studied by Maxwell [Maxwell  
95 1864]; a unifying view on polyhedral surfaces, compressive forces  
96 and corresponding “convex” force diagrams is presented by [Ash  
97 et al. 1988]. F. Fraternali [2002], [2010] established a connection  
98 between the continuous theory of stresses in membranes and the  
99 discrete theory of forces in thrust networks, by interpreting the lat-  
100 ter as a non-conforming finite element discretization of the former.

101 Several authors have studied the problem of finding discrete com-  
102 pressive force networks contained within the boundary of masonry  
103 structures; previous work in this area includes [O’Dwyer 1998] and  
104 [Andreu et al. 2007]. Fraternali [2010] proposed solving for the  
105 structure’s discrete stress surface, and examining its convex hull to  
106 study the structure’s stability and susceptibility to cracking.

107 Philippe Block’s seminal thesis introduced *Thrust Network Analy-*  
108 *sis*, which pioneered the use of thrust networks and their reciprocal  
109 diagrams for efficient and practical design of self-supporting ma-  
sonry structures. By first seeking a reciprocal diagram of the top  
110 view, guaranteeing equilibrium of horizontal forces, then solving  
111 for the heights that balance the vertical loads, Thrust Network Anal-  
112 ysis linearizes the form-finding problem. For a thorough overview  
113 of this methodology, see e.g. [Block and Ochsendorf 2007; Block  
114 2009]. Recent work by Block and coauthors extends this method  
115 in the case where the reciprocal diagram is not unique; for different  
116 choices of reciprocal diagram, the optimal heights can be found us-  
117 ing the method of least squares [Van Mele and Block 2011], and the  
118 search for the best such reciprocal diagram can be automated using  
119 a genetic algorithm [Block and Lachauer 2011].

120 Other approaches to the interactive design of self-supporting struc-  
121 tures include modeling these structures as damped particle-spring  
122 systems [Kilian and Ochsendorf 2005; Barnes 2009], and mirroring  
123 the rich tradition in architecture of designing self-supporting  
124 surfaces using hanging chain models [Heyman 1998]. Alterna-  
125 tively, masonry structures can be represented by networks of rigid

127 blocks [Livesley 1992], whose conditions on the structural feasibil-  
128 ity were incorporated into procedural modeling of buildings [Whit-  
129 ing et al. 2009].

130 Algorithmic and mathematical methods relevant to this paper are  
131 work on the geometry of quad meshes with planar faces [Glymph  
132 et al. 2004; Liu et al. 2006], discrete curvatures for such meshes  
133 [Pottmann et al. 2007; Bobenko et al. 2010], in particular curva-  
134 tures in isotropic geometry [Pottmann and Liu 2007]. Schiftner and  
135 Balzer [2010] discuss approximating a reference surface by a quad  
136 mesh with planar faces, whose layout is guided by statics properties  
137 of that surface.

138 

## 2 Self-supporting Surfaces

139 This section is the theoretical basis of the paper. §2.1 and §2.2 ex-  
140 plain the mathematical model for unsupported masonry and its dis-  
141 cretization, which is needed in our modeling algorithms. The con-  
142 nection with isotropic geometry (§2.3 and §2.4) is important for the  
143 later Section 5, which deals with self-supporting PQ meshes and  
144 moment-free steel/glass constructions. Finally §2.5 deals with the  
145 question how faithful our discretizations are.

146 

### 2.1 The Continuous Theory

147 We model masonry as a surface given by a height field  $s(x, y)$  de-  
148 fined in some planar domain  $\Omega$ . We assume that there are vertical  
149 loads  $F(x, y)$  — usually  $F$  represents the structure’s own weight.  
150 By definition this surface is self-supporting if and only if there ex-  
151 ist a field of compressive stresses which are in equilibrium with  
152 the acting forces. This is equivalent to existence of a field  $M(x, y)$   
153 of  $2 \times 2$  symmetric positive semidefinite matrices satisfying

$$\text{div}(M\nabla s) = F, \quad \text{div } M = 0, \quad (1)$$

154 where the divergence operator  $\text{div} \begin{pmatrix} u(x,y) \\ v(x,y) \end{pmatrix} = u_x + v_y$  is under-  
155 stood to act on the columns of a matrix (see e.g. [Fraternali 2010],  
156 [Giaquinta and Giusti 1985]).

157 The condition  $\text{div } M = 0$  says that  $M$  is locally the Hessian of a  
158 real-valued function  $\phi$  (the *Airy stress potential*): With the notation

$$M = \begin{pmatrix} m_{11} & m_{12} \\ m_{12} & m_{22} \end{pmatrix} \iff \widehat{M} = \begin{pmatrix} m_{22} & -m_{12} \\ -m_{12} & m_{11} \end{pmatrix}$$

159 it is clear that  $\text{div } M = 0$  is an integrability condition for  $\widehat{M}$ , so  
160 locally there is a potential  $\phi$  with

$$\widehat{M} = \nabla^2\phi, \quad \text{i.e.,} \quad M = \widehat{\nabla^2\phi}.$$

161 If the domain  $\Omega$  is simply connected, this relation holds globally.  
162 Positive semidefiniteness of  $M$  (or equivalently of  $\widehat{M}$ ) character-  
163 izes *convexity* of the Airy potential  $\phi$ . The Airy function enters  
164 computations only by way of its derivatives, so global existence is  
165 not an issue.

166 *Remark:* Stresses at boundary points depend on the way the sur-  
167 face is anchored: A fixed anchor means no condition, but a free  
168 boundary with outer normal vector  $\mathbf{n}$  means  $\langle M\nabla s, \mathbf{n} \rangle = 0$ .

169 **Stress Laplacian.** Note that  $\text{div } M = 0$  yields  $\text{div}(M\nabla s) =$   
170  $\text{tr}(M\nabla^2 s)$ , which we like to call  $\Delta_\phi s$ . The operator  $\Delta_\phi$  is sym-  
171 metric. It is elliptic (as a Laplace operator should be) if and only if  
172  $M$  is positive definite, i.e.,  $\phi$  is strictly convex. The balance condi-  
173 tion (1) may be written as  $\Delta_\phi s = F$ .

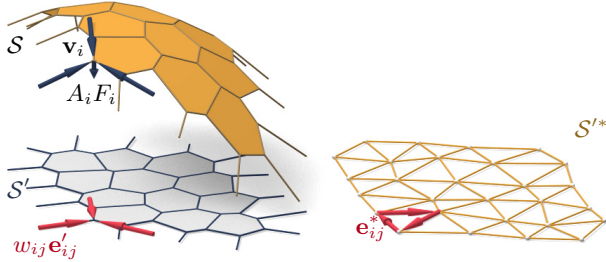


**Figure 2:** A thrust network  $\mathcal{S}$  with dangling edges indicating external forces (left). This network together with compressive forces which balance vertical loads  $A_i F_i$  projects onto a planar mesh  $\mathcal{S}'$  with equilibrium compressive forces  $w_{ij} \mathbf{e}'_{ij}$  in its edges. Rotating forces by  $90^\circ$  leads to the reciprocal force diagram  $\mathcal{S}'^*$  (right).

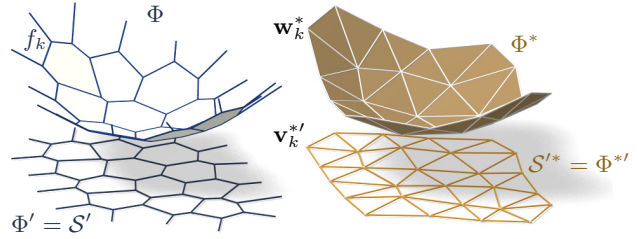


**Figure 3:** Airy stress potential  $\Phi$  and its polar dual  $\Phi^*$ .  $\Phi$  projects onto the same planar mesh as  $\mathcal{S}$  does, while  $\Phi^*$  projects onto the reciprocal force diagram. A primal face  $f_k$  lies in the plane  $z = \alpha x + \beta y + \gamma \iff$  the corresponding dual vertex is  $\mathbf{w}_k^* = (\alpha, \beta, -\gamma)$ .

## 2.2 Discrete Theory: Thrust Networks

We discretize a self-supporting surface by a mesh  $\mathcal{S} = (V, E, F)$  (see Figure 2). Loads are again vertical, and we discretize them as force densities  $F_i$  associated with vertices  $\mathbf{v}_i$ . The load acting on this vertex is then given by  $F_i A_i$ , where  $A_i$  is an area of influence (using a prime to indicate projection onto the  $xy$  plane,  $A_i$  is the area of the Voronoi cell of  $\mathbf{v}'_i$  w.r.t.  $V'$ ). We assume that stresses are carried by the edges of the mesh: the force exerted on the vertex  $\mathbf{v}_i$  by the edge connecting  $\mathbf{v}_i, \mathbf{v}_j$  is given by

$$w_{ij}(\mathbf{v}_j - \mathbf{v}_i), \quad \text{where } w_{ij} = w_{ji} \geq 0.$$

The nonnegativity of the individual weights  $w_{ij}$  expresses the compressive nature of forces. The balance conditions at vertices then read as follows: With  $\mathbf{v}_i = (x_i, y_i, s_i)$  we have

$$\sum_{j \sim i} w_{ij}(x_j - x_i) = \sum_{j \sim i} w_{ij}(y_j - y_i) = 0, \quad (2)$$

$$\sum_{j \sim i} w_{ij}(s_j - s_i) = A_i F_i. \quad (3)$$

A mesh equipped with edge weights in this way is a discrete *thrust network*. Invoking the safe theorem, we can state that a masonry structure is self-supporting, if we can find a thrust network with compressive forces which is entirely contained within the structure.

**Reciprocal Diagram.** Equations (2) have a geometric interpretation: with edge vectors

$$\mathbf{e}'_{ij} = \mathbf{v}'_j - \mathbf{v}'_i = (x_j, y_j) - (x_i, y_i),$$

Equation (2) asserts that vectors  $w_{ij} \mathbf{e}'_{ij}$  form a closed cycle. Rotating them by 90 degrees, we see that likewise

$$\mathbf{e}'_{ij}^* = w_{ij} J \mathbf{e}'_{ij}, \quad \text{with } J = \begin{pmatrix} 0 & -1 \\ 1 & 0 \end{pmatrix},$$

form a closed cycle (see Figure 2). If the mesh  $\mathcal{S}$  is simply connected, there exists an entire *reciprocal diagram*  $\mathcal{S}'^*$  which is a combinatorial dual of  $\mathcal{S}$ , and which has edge vectors  $\mathbf{e}'_{ij}^*$ . Its vertices are denoted by  $\mathbf{v}'_i^*$ .

**Remark:** If  $\mathcal{S}'$  is a Delaunay triangulation, then the corresponding Voronoi diagram is an example of a reciprocal diagram.

**Polyhedral Stress Potential.** We can go further and construct a convex polyhedral “Airy stress potential” surface  $\Phi$  with vertices  $\mathbf{w}_i = (x_i, y_i, \phi_i)$  combinatorially equivalent to  $\mathcal{S}$  by requiring that a primal face of  $\Phi$  lies in the plane  $z = \alpha x + \beta y + \gamma$  if and only if

$(\alpha, \beta)$  is the corresponding dual vertex of  $\mathcal{S}'^*$  (see Figure 3). Obviously this condition determines  $\Phi$  up to vertical translation. For existence see [Ash et al. 1988]. The inverse procedure constructs a reciprocal diagram from  $\Phi$ . This procedure works also if forces are not compressive: we can construct an Airy mesh  $\Phi$  which has planar faces, but it will no longer be a convex polyhedron.

The vertices of  $\Phi$  can be interpolated by a piecewise-linear function  $\phi(x, y)$ . It is easy to see that the derivative of  $\phi(x, y)$  jumps by the amount  $\|\mathbf{e}'_{ij}^*\| = w_{ij} \|\mathbf{e}'_{ij}\|$  when crossing over the edge  $\mathbf{e}'_{ij}$  at right angle, with unit speed. This identifies  $\Phi$  as the Airy polyhedron introduced by [Fraternali et al. 2002] as a finite element discretization of the continuous Airy function (see also [Fraternali 2010]).

If the mesh is not simply connected, the reciprocal diagram and the Airy polyhedron exist only locally. Our computations do not require global existence.

**Polarity.** Polarity with respect to the *Maxwell paraboloid*  $z = \frac{1}{2}(x^2 + y^2)$  maps the plane  $z = \alpha x + \beta y + \gamma$  to the point  $(\alpha, \beta, -\gamma)$ . Thus, applying polarity to  $\Phi$  and projecting the result  $\Phi^*$  into the  $xy$  plane reconstructs the reciprocal diagram  $\Phi'^* = \mathcal{S}'^*$  (see Fig. 3).

**Discrete Stress Laplacian.** The weights  $w_{ij}$  may be used to define a graph Laplacian  $\Delta_\phi$  which on vertex-based functions acts as

$$\Delta_\phi s(\mathbf{v}_i) = \sum_{j \sim i} w_{ij}(s_j - s_i).$$

This operator is a perfect discrete Laplacian in the sense of [Wardetzky et al. 2007], since it is symmetric by construction, Equation (2) implies linear precision for the planar “top view mesh”  $\mathcal{S}'$  (i.e.,  $\Delta_\phi f = 0$  if  $f$  is a linear function), and  $w_{ij} \geq 0$  ensures semidefiniteness and a maximum principle for  $\Delta_\phi$ -harmonic functions. Equation (3) can be written as  $\Delta_\phi s = AF$ .

Note that  $\Delta_\phi$  is well defined even when the underlying meshes are not simply connected.

## 2.3 Surfaces in Isotropic Geometry

It is worthwhile to reconsider the basics of self-supporting surfaces in the language of dual-isotropic geometry, which takes place in  $\mathbb{R}^3$  with the  $z$  axis as a distinguished vertical direction. The basic elements of this geometry are planes, having equation  $z = f(x, y) = \alpha x + \beta y + \gamma$ . The gradient vector  $\nabla f = (\alpha, \beta)$  determines the plane up to translation. A plane tangent to the graph of the function  $s(x, y)$  has gradient vector  $\nabla s$ .

There is the notion of *parallel points*:  $(x, y, z) \parallel (x', y', z') \iff x = x', y = y'$ .

243 **Remark:** The Maxwell paraboloid is considered the unit sphere of  
244 isotropic geometry, and the geometric quantities considered above  
245 are assigned specific meanings: The forces  $\|\mathbf{e}_{ij}^*\| = w_{ij}\|\mathbf{e}_{ij}\|$  are  
246 dihedral angles of the Airy polyhedron  $\Phi$ , and also “lengths” of  
247 edges of  $\Phi^*$ . We do not use this terminology in the sequel.

248 **Curvatures.** Generally speaking, in the differential geometry of  
249 surfaces one considers the *Gauss map*  $\sigma$  from a surface  $S$  to a con-  
250 vex unit sphere  $\Phi$  by requiring that corresponding points have par-  
251 allel tangent planes. Subsequently mean curvature  $H^{\text{rel}}$  and Gaus-  
252 sian curvature  $K^{\text{rel}}$  relative to  $\Phi$  are computed from the derivative  
253  $d\sigma$ . Classically  $\Phi$  is the ordinary unit sphere  $x^2 + y^2 + z^2 = 1$ , so  
254 that  $\sigma$  maps each point to its unit normal vector.

255 In our setting, parallelity is a property of *points* rather than planes,  
256 and the Gauss map  $\sigma$  goes the other way, mapping the tangent  
257 planes of the unit sphere  $z = \phi(x, y)$  to the corresponding tan-  
258 gent plane of the surface  $z = s(x, y)$ . If we know which point  
259 a plane is attached to, then the Gauss map is determined by the  
260 plane’s gradient. So we simply write

$$\nabla\phi \xrightarrow{\sigma} \nabla s.$$

261 By moving along a curve  $\mathbf{u}(t) = (x(t), y(t))$  in the parameter  
262 domain we get the first variation of tangent planes:  $\frac{d}{dt}\nabla\phi|_{\mathbf{u}(t)} =$   
263  $(\nabla^2\phi)\dot{\mathbf{u}}$ . This yields the derivative  $(\nabla^2\phi)\dot{\mathbf{u}} \xrightarrow{d\sigma} (\nabla^2s)\dot{\mathbf{u}}$ , for all  
264  $\dot{\mathbf{u}}$ , and the matrix of  $d\sigma$  is found as  $(\nabla^2\phi)^{-1}(\nabla^2s)$ . By definition,  
265 curvatures of the surface  $s$  relative to  $\phi$  are found as

$$K_s^{\text{rel}} = \det(d\sigma) = \frac{\det \nabla^2 s}{\det \nabla^2 \phi},$$

$$H_s^{\text{rel}} = \frac{1}{2} \text{tr}(d\sigma) = \frac{1}{2} \text{tr} \left( \frac{M}{\det \nabla^2 \phi} \nabla^2 s \right) = \frac{\Delta_\phi s}{2 \det \nabla^2 \phi}.$$

266 The Maxwell paraboloid  $\phi_0(x, y) = \frac{1}{2}(x^2 + y^2)$  is the canonical  
267 unit sphere of isotropic geometry, with Hessian  $E_2$ . Curvatures rel-  
268 ative to  $\phi_0$  are not called “relative” and are denoted by the symbols  
269  $H, K$  instead of  $H^{\text{rel}}, K^{\text{rel}}$ . The observation

$$\Delta_\phi \phi = \text{tr}(M \nabla^2 \phi) = \text{tr}(\widehat{\nabla^2 \phi} \nabla^2 \phi) = 2 \det \nabla^2 \phi$$

270 together with the formulas above implies

$$K_s = \det \nabla^2 s, \quad K_\phi = \det \nabla^2 \phi \implies H_s^{\text{rel}} = \frac{\Delta_\phi s}{2K_\phi} = \frac{\Delta_\phi s}{\Delta_\phi \phi}.$$

271 **Relation to Self-supporting Surfaces.** Summarizing the for-  
272 mulas above, we rewrite the balance condition (1) as

$$2K_\phi H_s^{\text{rel}} = \Delta_\phi s = F. \quad (4)$$

273 Let us draw some conclusions:

- Since  $H_\phi^{\text{rel}} = 1$  we see that the load  $F_\phi = 2K_\phi$  is admissible for the stress surface  $\phi(x, y)$ , which is hereby shown as self-supporting. The quotient of loads yields  $H_s^{\text{rel}} = F/F_\phi$ .
- If the stress surface coincides with the Maxwell paraboloid, then *constant loads characterize constant mean curvature surfaces*, because we get  $K_\phi = 1$  and  $H_s = F/2$ .
- If  $s_1, s_2$  have the same stress potential  $\phi$ , then  $H_{s_1-s_2}^{\text{rel}} = H_{s_1}^{\text{rel}} - H_{s_2}^{\text{rel}} = 0$ , so  $s_1 - s_2$  is a (relative) minimal surface.

## 2.4 Meshes in Isotropic Geometry

283 A general theory of curvatures of polyhedral surfaces with respect  
284 to a polyhedral unit sphere was proposed by [Pottmann et al. 2007;

285 Bobenko et al. 2010], and its dual complement in isotropic geo-  
286 metry was elaborated on in [Pottmann and Liu 2007]. As illustrated by  
287 Figure 4, the mean curvature of a self-supporting surface  $S$  relative  
288 to its discrete Airy stress potential is associated with the vertices of  
289  $S$ . It is computed from areas and mixed areas of faces in the polar  
290 polyhedra  $S^*$  and  $\Phi^*$ :

$$H^{\text{rel}}(\mathbf{v}_i) = \frac{A_i(S, \Phi)}{A_i(\Phi, \Phi)}, \quad \text{where}$$

$$A_i(S, \Phi) = \frac{1}{4} \sum_{k: f_k \in \text{1-ring}(\mathbf{v}_i)} \det(\mathbf{v}'_k, \mathbf{w}'_{k+1}) + \det(\mathbf{w}'_k, \mathbf{v}'_{k+1}).$$

The prime denotes the projection into the  $xy$  plane, and summation  
is over those dual vertices which are adjacent to  $\mathbf{v}_i$ . Replacing  $\mathbf{v}'_k$   
by  $\mathbf{w}'_k$  yields  $A_i(\Phi, \Phi) = \frac{1}{2} \sum \det(\mathbf{w}'_k, \mathbf{w}'_{k+1})$ .

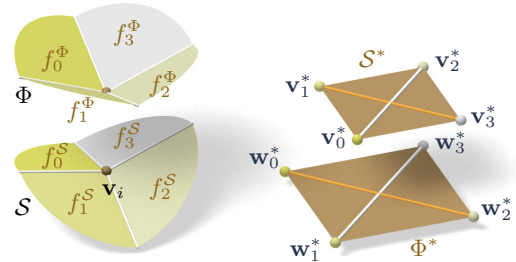


**Figure 4:** Mean curvature of a vertex  $\mathbf{v}_i$  of  $S$ : Corresponding edges of the polar duals  $S^*$ ,  $\Phi^*$  are parallel, and mean curvature according to [Pottmann et al. 2007] is computed from the vertices polar to faces adjacent to  $\mathbf{v}_i$ . For valence 4 vertices the case of zero mean curvature shown here is characterized by parallelity of non-corresponding diagonals of corresponding quads in  $S^*$ ,  $\Phi^*$ .

**Proposition.** If  $\Phi$  is the Airy surface of a thrust network  $S$ , then the mean curvature of  $S$  relative to  $\Phi$  is computable as

$$H^{\text{rel}}(\mathbf{v}_i) = \frac{\sum_{j \sim i} w_{ij}(s_j - s_i)}{\sum_{j \sim i} w_{ij}(\phi_j - \phi_i)} = \frac{\Delta_\phi s}{\Delta_\phi \phi}|_{\mathbf{v}_i}. \quad (5)$$

**Proof.** It is sufficient to show  $2A_i(S, \Phi) = \sum_{j \sim i} w_{ij}(s_j - s_i)$ .

For that, consider edges  $\mathbf{e}'_1, \dots, \mathbf{e}'_n$  emanating from  $\mathbf{v}'_i$ . The dual cycles in  $\Phi'^*$  and  $S'^*$  without loss of generality are given by vertices  $(\mathbf{v}'_1, \dots, \mathbf{v}'_n)$  and  $(\mathbf{w}'_1, \dots, \mathbf{w}'_n)$ , respectively. The latter has edges  $\mathbf{w}'_{j+1} - \mathbf{w}'_j = w_{ij} J \mathbf{e}'_j$  (indices modulo  $n$ ).

Without loss of generality  $\mathbf{v}_i = 0$ , so the vertex  $\mathbf{v}'_j$  by construction equals the gradient of the linear function  $\mathbf{x} \mapsto \langle \mathbf{v}'_j, \mathbf{x} \rangle$  defined by the properties  $\mathbf{e}'_{j-1} \mapsto s_{j-1} - s_i$ ,  $\mathbf{e}'_j \mapsto s_j - s_i$ . Corresponding edge vectors  $\mathbf{v}'_{j+1} - \mathbf{v}'_j$  and  $\mathbf{w}'_{j+1} - \mathbf{w}'_j$  are parallel, because  $\langle \mathbf{v}'_{j+1} - \mathbf{v}'_j, \mathbf{e}'_j \rangle = (s_j - s_i) - (s_j - s_i) = 0$ . Expand  $2A_i(S, \Phi)$ :

$$\begin{aligned} & \frac{1}{2} \sum \det(\mathbf{w}'_j, \mathbf{v}'_{j+1}) + \det(\mathbf{v}'_j, \mathbf{w}'_{j+1}) \\ &= \frac{1}{2} \sum \det(\mathbf{w}'_j - \mathbf{w}'_{j+1}, \mathbf{v}'_{j+1}) + \det(\mathbf{v}'_j, \mathbf{w}'_{j+1} - \mathbf{w}'_j) \\ &= \frac{1}{2} \sum \det(-w_{ij} J \mathbf{e}'_j, \mathbf{v}'_{j+1}) + \det(\mathbf{v}'_j, w_{ij} J \mathbf{e}'_j) \\ &= \sum \det(\mathbf{v}'_j, w_{ij} J \mathbf{e}'_j) = \sum w_{ij} \langle \mathbf{v}'_j, \mathbf{e}'_j \rangle = \sum w_{ij} (s_j - s_i). \end{aligned}$$

Here we have used  $\det(\mathbf{a}, J\mathbf{b}) = \langle \mathbf{a}, \mathbf{b} \rangle$ .  $\square$

In order to discretize (4), we also need a discrete Gaussian curvature, usually defined as a quotient of areas which correspond under the Gauss mapping. We define

$$K_\Phi(\mathbf{v}_i) = \frac{A_i(\Phi, \Phi)}{A_i},$$

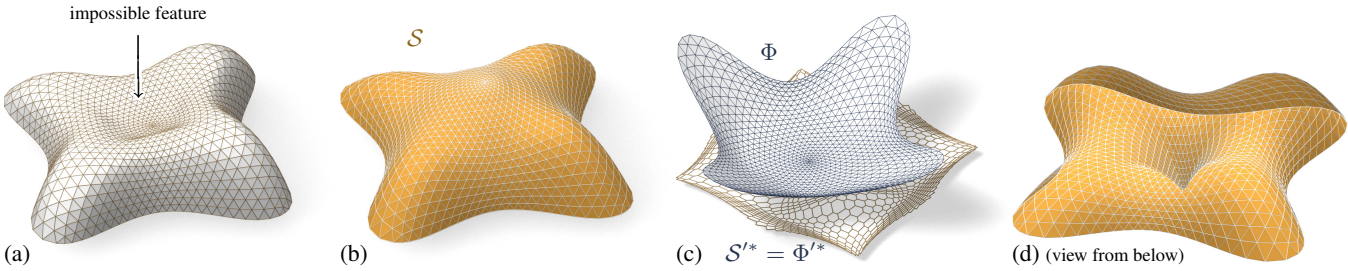


**Figure 5:** The top of the Lilium Tower (a) cannot stand as a masonry structure, because its central part is concave. Our algorithm finds a nearby self-supporting mesh (b) without this impossible feature. (c) shows the corresponding Airy mesh  $\Phi$  and reciprocal force diagram  $S'^*$ . (d) The user can edit the original surface, such as by specifying that the center of the surface is supported by a vertical pillar, and the self-supporting network adjusts accordingly.

where  $A_i$  is the Voronoi area of vertex  $v'_i$  in the projected mesh  $S'$  used in (3).

*Remark:* If the faces of the thrust network  $S$  are not planar, the simple trick of introducing additional edges with zero forces in them makes them planar, and the theory is applicable. In the interest of space, we refrain from elaborating further.

**Discrete Balance Equation.** The discrete version of the balance equation (4) reads as follows:

**Theorem.** A simply-connected mesh  $S$  with vertices  $v_i = (x_i, y_i, s_i)$  can be put into static equilibrium with vertical nodal forces  $A_i F_i$  if and only if there exists a combinatorially equivalent mesh  $\Phi$  with planar faces and vertices  $(x_i, y_i, \phi_i)$ , such that curvatures of  $S$  relative to  $\Phi$  obey

$$2K_\Phi(v_i)H^{\text{rel}}(v_i) = F_i \quad (6)$$

at every interior vertex and every free boundary vertex  $v_i$ .  $S$  can be put into compressive static equilibrium if and only if there exists a convex such  $\Phi$ .

*Proof.* The relation between equilibrium forces  $w_{ij}e_{ij}$  in  $S$  and the polyhedral stress potential  $\Phi$  has been discussed above, and so has the equivalence “ $w_{ij} \geq 0 \iff \Phi$  convex” (see e.g. [Ash et al. 1988] for a survey of this and related results). It remains to show that Equations (2) and (6) are equivalent. This is the case because the proposition above implies  $2K(v_i)H^{\text{rel}}(v_i) = 2\frac{A_i(\Phi, \Phi)}{A_i} \frac{A_i(\Phi, S)}{A_i(\Phi, \Phi)} = \frac{1}{A_i}(\sum_{j \sim i} w_{ij}(s_j - s_i)) = \frac{1}{A_i} A_i F_i$ .  $\square$

## 2.5 Convergence

When considering discrete thrust networks as discretizations of continuous self-supporting surfaces, the following question is important: For a given smooth surface  $s(x, y)$  with Airy stress function  $\phi$ , does there exist a polyhedral surface  $S$  in equilibrium approximating  $s(x, y)$ , whose top view is a given planar mesh  $S'$ ? We restrict our attention to triangle meshes, where planarity of the faces of the discrete stress surface  $\Phi$  is not an issue. This question has several equivalent reformulations:

- Does  $S'$  have a reciprocal diagram whose corresponding Airy polyhedron  $\Phi$  approximates the continuous Airy potential  $\phi$ ? (if the surfaces involved are not simply connected, these objects are defined locally).
- Does  $S'$  possess a “perfect” discrete Laplace-Beltrami operator  $\Delta_\phi$  in the sense of Wardetzky et al. [2007] whose weights are the edge length scalars of such a reciprocal diagram?

From [Wardetzky et al. 2007] we know that perfect Laplacians exist only on regular triangulations which are projections of convex polyhedra. On the other hand, previous sections show how to appropriately re-triangulate: Let  $\Phi$  be a triangle mesh convex hull of the vertices  $(x_i, y_i, \phi(x_i, y_i))$ , where  $(x_i, y_i)$  are vertices of  $S'$ . Then its polar dual  $\Phi^*$  projects onto a reciprocal diagram with positive edge weights, so  $\Delta_\phi$  has positive weights, and the vertices  $(x_i, y_i, s_i)$  of  $S$  can be found by solving the discrete Poisson problem  $(\Delta_\phi s)_i = A_i F_i$ .

We expect, but we don’t prove, that the discrete  $\Delta_\phi$  approximates its continuous counterpart for reasonable sampling (after all it is directly derived from  $\phi(x, y)$ ). This implies that solving the discrete Poisson equation leads to a mesh approximating its continuous counterpart  $s(x, y)$ , and we have convergence as the sampling density increases. A rigorous analysis is a topic for future research.

## 3 Thrust Networks from Reference Meshes

Consider now the problem of taking a given reference mesh, say  $R$ , and finding a combinatorially equivalent mesh  $S$  in static equilibrium approximating  $R$ . The loads on  $S$  include user-prescribed loads as well as the dead load caused by the mesh’s own weight. Conceptually, finding  $S$  amounts to minimizing some formulation of distance between  $R$  and  $S$ , subject to constraints (2), (3), and  $w_{ij} \geq 0$ . For any choice of distance this minimization will be a nonlinear, non-convex, inequality-constrained variational problem. Our experience with black-box solvers [Wächter and Biegler 2006] is that they perform well for surfaces without complex geometry or for polishing reference meshes close to self-supporting, but fail to converge in reasonable time for more complicated shapes such as the one of Fig. 1, left. We therefore propose the following specialized, staggered linearization for solving the optimization problem:

0. Start with an initial guess  $S = R$ .
1. Estimate the self-load on the vertices of  $S$ , using their current positions.
2. Fixing  $S$ , locally fit an associated stress surface  $\Phi$ .
3. Alter positions  $v_i$  to improve the fit.
4. Repeat from Step 1 until convergence.

*Remark:* This staggered approach shares the several advantages of solving the full nonlinear problem: a nearby self-supporting surface is found given only a suggested reference shape, without needing to single one of the many possible top view reciprocal diagrams or needing to specify boundary tractions – these are found automatically during optimization. Although providing an initial top view graph with good combinatorics remains important, by not fixing the top view our approach allows the thrust network to slide both vertically and tangentially to the ground, essential to finding faithful thrust networks for surfaces with free boundary conditions.

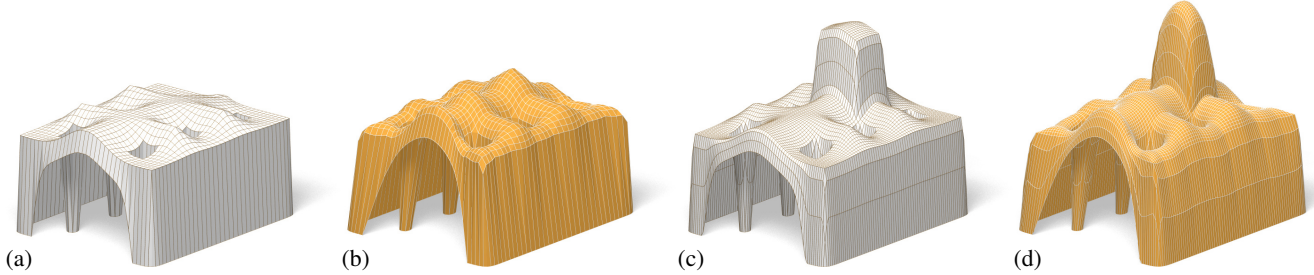


**Figure 6:** The user-designed reference mesh (a) is not self-supporting, but our algorithm finds a nearby perturbation of the reference surface (b) that is in equilibrium. As the user makes edits to the reference surface (c), the thrust network automatically adjusts (d).

**Step 1: Estimating Self-Load.** The dead load due to the surface’s own weight depends not only on the top view of  $\mathcal{S}$ , but also on the surface area of its faces. To avoid adding nonlinearity to the algorithm, we estimate the load coefficients  $F_i$  at the beginning of each iteration, and assume they remain constant until the next iteration. We estimate the load  $A_i F_i$  associated with each vertex by calculating its Voronoi surface area on each of its incident faces (note that this surface area is distinct from  $A_i$ , the vertex’s Voronoi area on the top view), and then multiplying by a user-specified surface density  $\rho$ .

**Step 2: Fit a Stress Surface.** In this step, we fix  $\mathcal{S}$  and try to fit a stress surface  $\Phi$  subordinate to the top view  $\mathcal{S}'$  of the primal mesh. We do so by searching for dihedral angles between the faces of  $\Phi$  which minimize, in the least-squares sense, the error in force equilibrium (6) and local integrability of  $\Phi$ . Doing so is equivalent to minimizing the squared residuals of Equations (3) and (2), with the positions held fixed. We define the *equilibrium energy*

$$E = \sum_i \left\| \begin{pmatrix} 0 \\ 0 \\ A_i F_i \end{pmatrix} - \sum_{j \sim i} w_{ij} (\mathbf{v}_j - \mathbf{v}_i) \right\|^2, \quad (7)$$

where  $i$  runs through interior and free boundary vertices, and solve

$$\min_{w_{ij}} E, \quad \text{s.t. } 0 \leq w_{ij} \leq w_{\max}. \quad (8)$$

Here  $w_{\max}$  is an optional maximum weight we are willing to assign (to limit the amount of stress in the surface). This convex, sparse, box-constrained least-squares problem [Friedlander 2007] always has a solution. If the objective is 0 at this solution, the faces of  $\Phi$  locally integrate to a stress surface satisfying (6), and this  $\Phi$  certifies that  $\mathcal{S}$  is self-supporting – we are done. Otherwise,  $\mathcal{S}$  is not self-supporting and its vertices must be moved.

**Step 3: Alter Positions.** In the previous step we fit as best as possible a stress surface  $\Phi$  to  $\mathcal{S}$ . There are two possible kinds of error with this fit: the faces around a vertex (equivalently, the reciprocal diagram) might not close up; and the resulting stress forces might not be exactly in equilibrium with the loads. These errors can be decreased by modifying the top view and heights of  $\mathcal{S}$ , respectively. It is possible to simply solve for new vertex positions that put  $\mathcal{S}$  in static equilibrium, since Equations (2) and (3) with  $w_{ij}$  fixed form a square linear system that is typically nonsingular.

While this approach would yield a self-supporting  $\mathcal{S}$ , this mesh is often far from the reference mesh  $\mathcal{R}$ , since any local errors in the stress surface from Step 2 amplify into global errors in  $\mathcal{S}$ . We propose instead to look for new positions that decrease the imbalance in the stresses and loads, while also penalizing drift away from the reference mesh:

$$\min_{\mathbf{v}} E + \alpha \sum_i \langle \mathbf{n}_i, \mathbf{v}_i - \mathbf{v}_i^0 \rangle^2 + \beta \|\mathbf{v} - \mathbf{v}_P^0\|^2,$$

Fig.	Vertices	Edges	Time (s)	Iterations	Max. Rel. Error
5b	1201	3504	21.6	9	$4.2 \times 10^{-5}$
5d	1200	3500	26.5	10	$8.5 \times 10^{-5}$
7	1535	2976	17.0	21	$2.7 \times 10^{-5}$
8	752	2165	8.0	9	$5.8 \times 10^{-5}$
11	2358	4302	19.5	9	$3.0 \times 10^{-4}$
16	527	998	5.7	25	$2.4 \times 10^{-5}$

**Table 1:** Numerical details about our examples. We show the clock time needed by an Intel Xeon 2.3GHz desktop PC with 4 GB of RAM to find a self-supporting thrust network and associated stress surface from the example’s reference mesh; we also give the number of outer iterations of the four steps in (§3). The maximum relative error is the dimensionless quantity  $\max_i \|A_i F_i - \sum_{j \sim i} w_{ij} (\mathbf{v}_j - \mathbf{v}_i)\| / \|A_i F_i\|$  (the maximum is taken over interior vertices  $\mathbf{v}_i$ ).

where  $\mathbf{v}_i^0$  is the position of the  $i$ -th vertex at the start of this step of the optimization,  $\mathbf{n}_i$  is the starting vertex normal (computed as the average of the incident face normals),  $\mathbf{v}_P^0$  is the projection of  $\mathbf{v}^0$  onto the reference mesh, and  $\alpha > \beta$  are penalty coefficients that are decreased every iteration of Steps 1–3. The second term allows  $\mathcal{S}$  to slide over itself (if doing so improves equilibrium) but penalizes drift in the normal direction. The third term, weaker than the second, regularizes the optimization by preventing large drift away from the reference surface or excessive tangential sliding.

**Implementation Details.** Solving the weighted least-squares problem of Step 3 amounts to solving a sparse, symmetric linear system. While the MINRES algorithm [Paige and Saunders 1975] is likely the most robust algorithm for solving this system, in practice we have observed that the method of conjugate gradients works well despite the potential ill-conditioning of the objective matrix.

**Limitations.** This algorithm is not guaranteed to always converge; this fact is not surprising from the physics of the problem (if the boundary of the reference mesh encloses too large of a region,  $w_{\max}$  is set too low, and the density of the surface too high, a thrust network in equilibrium simply does not exist – the vault is too ambitious and cannot be built to stand; pillars are needed.)

We can, however, make a few remarks. Only Step 1 can increase the equilibrium energy  $E$  of Equation (7). Step 2 always decreases it, and Step 3 does as well as  $\beta \rightarrow 0$ . Moreover, as  $\alpha \rightarrow 0$  and  $\beta \rightarrow 0$ , Step 3 approaches a linear system with as many equations as unknowns; if this system has full rank, its solution sets  $E = 0$ . These facts suggest that the algorithm should generally converge to a thrust network in equilibrium, provided that Step 1 does not increase the loads by too much at every iteration, and this is indeed what we observe in practice. One case where this assumption is

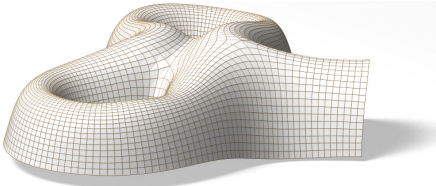


**Figure 7:** A freeform surface (left) needs adjustments around the entrance arch and between the two pillars in order to be self-supporting; our algorithm finds the nearby surface in equilibrium (right) that incorporates these changes.

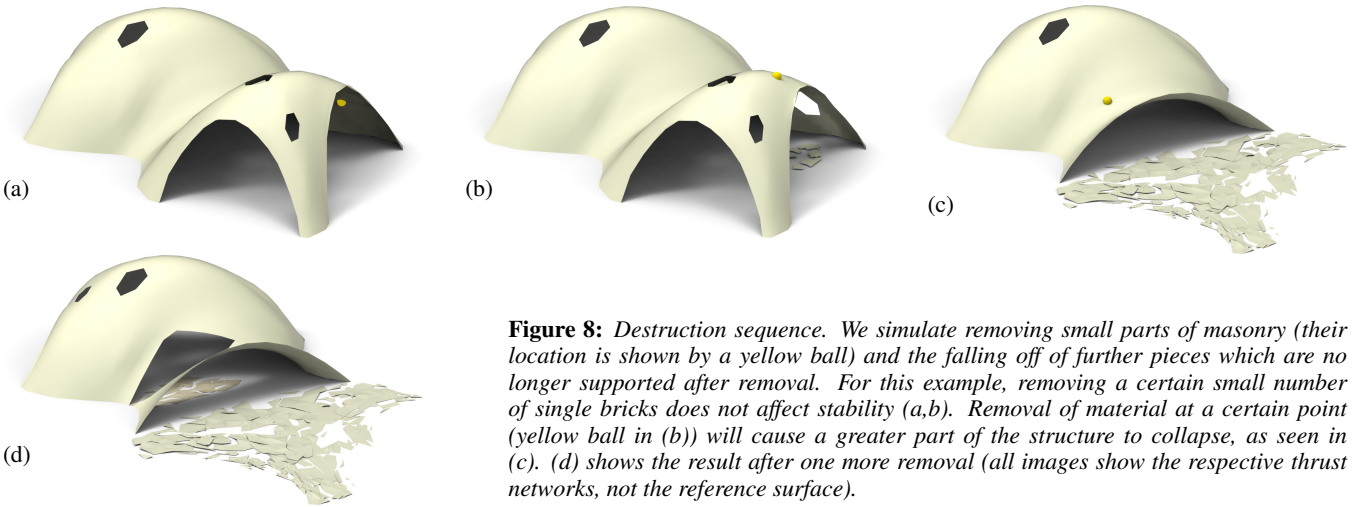


**Figure 8:** Destruction sequence. We simulate removing small parts of masonry (their location is shown by a yellow ball) and the falling off of further pieces which are no longer supported after removal. For this example, removing a certain small number of single bricks does not affect stability (a,b). Removal of material at a certain point (yellow ball in (b)) will cause a greater part of the structure to collapse, as seen in (c). (d) shows the result after one more removal (all images show the respective thrust networks, not the reference surface).

guaranteed to hold is if the thickness of the surface is allowed to freely vary, so that it can be chosen so that the surface has uniform density over the top view.

If the linear system in Step 3 is singular and infeasible, the algorithm can stall at  $E > 0$ . This failure occurs, for instance, when an interior vertex has height  $z_i$  lower than all of its neighbors, and Step 2 assigns all incident edges to that vertex a weight of zero: clearly no amount of moving the vertex or its neighbors can bring the vertex into equilibrium. We avoid such degenerate configurations by bounding weights slightly away from zero in (8), trading increased robustness for slight smoothing of the resulting surface. Attempting to optimize meshes that have self-intersecting top views (i.e., aren't height fields), have too many impossible features, or are insufficiently supported by fixed boundary points can also result in errors and instability.

## 4 Results

**Interactive Design of Self-Supporting Surfaces.** The optimization algorithm described in the previous section forms the basis of an interactive design tool for self-supporting surfaces. Users manipulate a mesh representing a reference surface, and the computer searches for a nearby thrust network in equilibrium (see e.g. Figure 6). Features of the design tool include:

- Handle-based 3D editing of the reference mesh using Laplacian coordinates [Lipman et al. 2004; Sorkine et al. 2003] to extrude vaults, insert pillars, and apply other deformations to the reference mesh. Handle-based adjustments of the heights, keeping the top view fixed, and deformation of the top view, keeping the heights fixed, are also supported. The thrust network adjusts interactively to fit the deformed positions, giving the usual visual feedback about the effects of edits on whether or not the surface can stand.
- Specification of boundary conditions. Points of contact be-

tween the reference surface and the ground or environment are specified by “pinning” vertices of the surface, specifying that the thrust network must coincide with the reference mesh at this point, and relaxing the condition that forces must be in equilibrium there.

- Interactive adjustment of surface density  $\rho$ , external loads, and maximum permissible stress per edge  $w_{\max}$ , with visual feedback of how these parameters affect the fitted thrust network.
- Upsampling of the thrust network through Catmull-Clark subdivision and polishing of the resulting refined thrust network using optimization (§3).
- Visualization of the stress surface dual to the thrust network and corresponding reciprocal diagram.

**Examples.** *Vault with Pillars:* As an example of the design and optimization workflow, consider a rectangular vault with six pillars, free boundary conditions along one edge, fixed boundary conditions along the others, and a tower extruded from the top of the surface (see Figure 6). This surface is neither convex nor simply connected, and exhibits a mix of boundary conditions, none of which cause our algorithm any difficulty; it finds a self-supporting thrust network near the designed reference mesh. The user is now free to make edits to the reference mesh, and the thrust network adapts to these edits, providing the user feedback on whether these designs are physically realizable.

*Example: Top of the Lilium Tower.* Consider the top portion of the steel-glass exterior surface of the Lilium Tower, which is currently being built in Warsaw (see Figure 5). What is if we had wanted to build this surface out of masonry instead? This surface contains a concave part with local minimum in its interior and so cannot possibly be self-supporting without modification. Given this surface as a reference mesh, our algorithm constructs a nearby thrust network in equilibrium without the impossible feature. The user can then

**Figure 9:** Stability Test. Left: Coloring and cross-section of edges visualize the magnitude of forces in a thrust network which is in equilibrium with this dome's dead load. Right: When an additional load is applied, there exists a corresponding compressive thrust network which is still contained in the masonry hull of the original dome. This implies stability of the dome under that load.

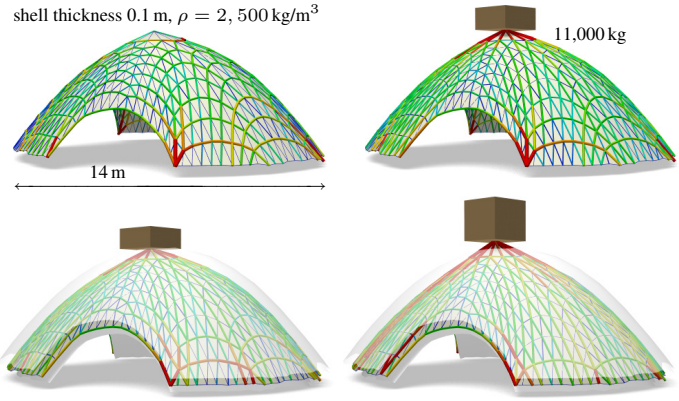


**Figure 10:** Stability test similar to Figure 9, but with a shell thickness of 1 m, in order to better visualize the way the thrust network starts to leave the masonry hull as the load increases. Additional loads are 0 kg, 5,000 kg, 10,000 kg, and 20,000 kg, resp., from left to right.

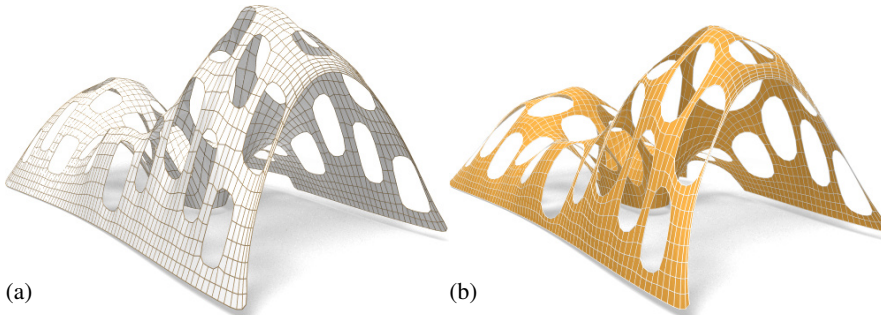


**Figure 11:** A mesh with holes (a) requires large deformations to both the top view and heights to render it self-supporting (b)

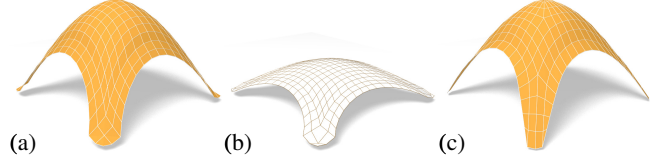


**Figure 12:** Directly enforcing planarity of the faces of even a very simple self-supporting quad-mesh vault (a) results in a surface far removed from the original design (b). Starting instead from a remeshing of the surface with edges following relative principal curvature directions yields a self-supporting, PQ mesh far more faithful to the original (c).

## 5 Special Self-Supporting Surfaces

**PQ Meshes.** Meshes with *planar* faces are of particular interest in architecture, so in this section we discuss how to remesh a given thrust network in equilibrium such that it becomes a quad mesh with planar faces (again in equilibrium). If this mesh is realized as a steel-glass construction, it is self-supporting in its beams alone, with no forces exerted on the glass (this is the usual manner of using glass). The beams constitute a self-supporting structure which is in perfect force equilibrium (without moments in the nodes) if only the deadload is applied.

Taking an arbitrary non-planar quad mesh and attempting naive, simultaneous enforcement of planarity and static equilibrium – either by staggering a planarity optimization step every outer iteration, or adding a planarity penalty term to the position update – does not yield good results, as shown in Figure 12. Indeed, as we will see later in this section, such a planar perturbation of a thrust network

530 explore how editing the reference mesh – adding a pillar, for example  
531 – affects the thrust network and its deviation from the reference  
532 surface.

533 **Example: Freeform Structure with Two Pillars.** Suppose an architect's experience and intuition has permitted the design of a nearly  
534 self-supporting freeform surface (Figure 7). Our algorithm reveals  
535 those edits needed to make the structure sound – principally around  
536 the entrance arch, and the area between the two pillars.  
537

538 **Example: Destruction Sequence.** In Figure 8 we simulate removing  
539 parts of masonry and the falling off of further pieces which are no  
540 longer supported after removal. This is done by deleting the 1-  
541 neighborhood of a vertex and solving for a new thrust network in  
542 compressive equilibrium close to the original reference surface. We  
543 delete those parts of the network which deviate too much and are  
544 no longer contained in the masonry hull, and iterate.

545 **Example: Stability Test:** See Figures 9 and 10 for a series of images  
546 which visualize the effect of additional loads on a thrust network.

547 **Example: Swiss Cheese.** Cutting holes in a self-supporting surface  
548 interrupts force flow lines and causes dramatic global changes to  
549 the surface stresses, often to the point that the surface is no longer  
550 in equilibrium. Whether a given surface with many such holes can  
551 stand is far from obvious. Figure 11a shows such an implausible  
552 and unstable surface; our optimization finds a nearby, equally im-  
553 plausible but stable surface without difficulty (see Figures 1, left  
554 and 11b).

555 **Example: Structural Glass.** See Figure 16 for details on a self-  
556 supporting surface which is realized not as masonry, but as a steel/  
557 glass construction with glass as a structural element.

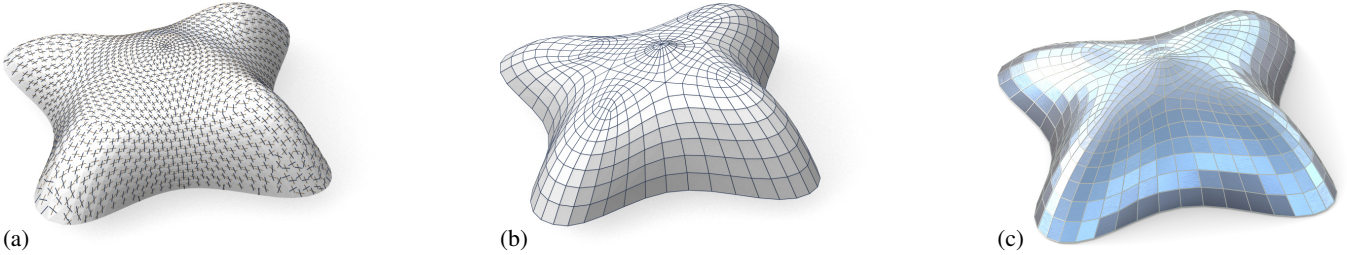


**Figure 13:** Planar quad remeshing of the surface of Fig. 5. (a) Relative principal directions, found from eigenvectors of  $(\nabla^2\phi)^{-1}\nabla^2s$ . (b) Quad mesh guided by principal directions is almost planar and almost self-supporting. (c) Small changes achieve both properties.

**Figure 14:** Planar quad remeshing of the surface of Figure 7. Left: Relative principal directions. Right: The result of optimization is a self-supporting PQ mesh, which guides a moment-free steel/glass construction (interior view, see also Fig. 1).



574 is not expected to generally exist.

575 Consider a planar quad mesh  $\mathcal{S}$  with vertices  $\mathbf{v}_{ij} = (x_{ij}, y_{ij}, s_{ij})$   
576 which approximates a given continuous surface  $s(x, y)$ . It is known  
577 that  $\mathcal{S}$  must approximately follow a network of conjugate curves in  
578 the surface (see e.g. [Liu et al. 2006]). We can derive this condition  
579 in an elementary way as follows: Using a Taylor expansion, we  
580 compute the volume of the convex hull of the quadrilateral  $\mathbf{v}_{ij},$   
581  $\mathbf{v}_{i+1,j}, \mathbf{v}_{i+1,j+1}, \mathbf{v}_{i,j+1}$ , assuming the vertices lie exactly on the  
582 surface  $s(x, y)$ . This results in

$$\text{vol} = \frac{1}{6} \det(\mathbf{a}_1, \mathbf{a}_2) \cdot ((\mathbf{a}_1)^T \nabla^2 s \mathbf{a}_2) + \dots,$$

where  $\mathbf{a}_1 = \begin{pmatrix} x_{i+1,j} - x_{ij} \\ y_{i+1,j} - y_{ij} \end{pmatrix}, \quad \mathbf{a}_2 = \begin{pmatrix} x_{i,j+1} - x_{ij} \\ y_{i,j+1} - y_{ij} \end{pmatrix},$

583 and the dots indicate higher order terms. We see that planarity re-  
584 quires  $(\mathbf{a}_1)^T \nabla^2 s \mathbf{a}_2 = 0$ . In addition to the mesh  $\mathcal{S}$  approximating  
585 the surface  $s(x, y)$ , the corresponding polyhedral Airy surface  $\Phi$   
586 must approximate  $\phi(x, y)$ ; thus we get the conditions

$$(\mathbf{a}_1)^T \nabla^2 s \mathbf{a}_2 = (\mathbf{a}_1)^T \nabla^2 \phi \mathbf{a}_2 = 0.$$

587  $\mathbf{a}_1, \mathbf{a}_2$  are therefore eigenvectors of  $(\nabla^2\phi)^{-1}\nabla^2s$ . In view of §2.3,  
588  $\mathbf{a}_1, \mathbf{a}_2$  indicate the principal directions of the surface  $s(x, y)$  rela-  
589 tive to  $\phi(x, y)$ .

590 In the discrete case, where  $s, \phi$  are not given as continuous surfaces,  
591 but are represented by a mesh in equilibrium and its Airy mesh, we  
592 use the techniques of Schiftner [2007] and Cohen-Steiner and Mor-  
593 van [2003] to approximate the Hessians  $\nabla^2s, \nabla^2\phi$ , compute prin-  
594 cipal directions as eigenvectors of  $(\nabla^2\phi)^{-1}\nabla^2s$ , and subsequently  
595 find meshes  $\mathcal{S}, \Phi$  approximating  $s, \phi$  which follow those directions.  
596 Global optimization can now polish  $\mathcal{S}, \Phi$  to a valid thrust network  
597 with discrete stress potential, where before it failed: we do so by  
598 taking the planarity energy  $\sum_f (2\pi - \theta_f)^2$ , where the sum runs  
599 over faces and  $\theta_f$  is the sum of the interior angles of face  $f$ , lin-  
600 earizing it at every iteration, and adding it to the objective function  
601 of the position update (Step 3). Convexity of  $\Phi$  ensures that  $\mathcal{S}$  is  
602 self-supporting.

603 Note that for each  $\Phi$ , the relative principal curvature directions give  
604 the *unique* curve network along which a planar quad discretization

605 of a self-supporting surface is possible. Other networks lead to re-  
606 sults like the one shown by Figure 12. Figures 13 and 14 further  
607 illustrate the result of applying this procedure to self-supporting  
608 surfaces.

609 *Remark:* When remeshing a given shape by planar quad meshes, we  
610 know that the circular and conical properties require that the mesh  
611 follows the ordinary, Euclidean principal curvature directions [Liu  
612 et al. 2006]. It is remarkable that the self-supporting property in a  
613 similar manner requires us to follow certain *relative* principal direc-  
614 tions. Practitioners' observations regarding the beneficial statics  
615 properties of principal directions can be explained by this analogy,  
616 because the relative principal directions are close to the Euclidean  
617 ones, if the stress distribution is uniform and  $\|\nabla s\|$  is small.

618 **Koenigs Meshes.** Given a self-supporting thrust network  $\mathcal{S}$  with  
619 stress surface  $\Phi$ , we ask the question: Which vertical perturbation  
620  $\mathcal{S} + \mathcal{R}$  is self-supporting, with the same loads as  $\mathcal{S}$ ? As to notation,  
621 all involved meshes  $\mathcal{S}, \mathcal{R}, \Phi$  have the same top view, and arithmetic  
622 operations refer to the respective  $z$  coordinates  $s_i, r_i, \phi_i$  of vertices.

623 The condition of equal loads then is expressed as  $\Delta_\phi(s + r) =$   
624  $\Delta_\phi s$  in terms of Laplacians or as  $H_{\mathcal{S}}^{\text{rel}} = H_{\mathcal{S} + \mathcal{R}}^{\text{rel}}$  in terms of mean  
625 curvature, and is equivalent to

$$\Delta_\phi r = 0, \quad \text{i.e.,} \quad H_{\mathcal{R}}^{\text{rel}} = 0.$$

626 So  $\mathcal{R}$  is a *minimal surface* relative to  $\Phi$ . While in the triangle mesh  
627 case there are enough degrees of freedom for nontrivial solutions,  
628 the case of planar quad meshes is more intricate: Polar polyhedra  
629  $\mathcal{R}^*, \Phi^*$  have to be Christoffel duals of each other [Pottmann and  
630 Liu 2007], as illustrated by Figure 4. Unfortunately not all quad  
631 meshes have such a dual; the condition is that the mesh is *Koenigs*,  
632 i.e., the derived mesh formed by the intersection points of diagonals  
633 of faces again has planar faces [Bobenko and Suris 2008].

634 **Koebe meshes.** An interesting special case occurs if  $\Phi$  is a  
635 *Koebe mesh* of isotropic geometry, i.e., a PQ mesh whose edges  
636 touch the Maxwell paraboloid. Since  $\Phi$  approximates the Maxwell  
637 paraboloid, we get  $2K(\mathbf{v}_i)H^{\text{rel}}(\mathbf{v}_i) \approx 1$  and  $\Phi$  consequently is



**Figure 15:** A “Koebe” mesh  $\Phi$  is self-supporting for unit dead load. An entire family of self-supporting meshes with the same top view is defined by  $\mathcal{S}_\alpha = \Phi + \alpha\mathcal{R}$ , where  $\mathcal{R}$  is chosen as  $\Phi$ ’s Christoffel-dual.

638 self-supporting for unit load. Applying the Christoffel dual con-  
639 struction described above yields a minimal mesh  $\mathcal{R}$  and a family of  
640 meshes  $\Phi + \alpha\mathcal{R}$  which are self-supporting for unit load (see Fig-  
641 ure 15).

## 6 Conclusion and Future Work

643 **Conclusion.** This paper builds on relations between statics and  
644 geometry, some of which have been known for a long time, and  
645 connects them with newer methods of discrete differential geo-  
646 metry, such as discrete Laplace operators and curvatures of polyhedral  
647 surfaces. We were able to find efficient ways of modeling self-  
648 supporting freeform shapes, and provide architects and engineers  
649 with an interactive tool for evaluating the statics of freeform  
650 geometries. The self-supporting property of a shape is directly re-  
651 relevant for freeform masonry. The actual thrust networks we use for  
652 computation are relevant e.g. for steel constructions, where equilib-  
653 rium of deadload forces implies absence of moments. This theory  
654 and accompanying algorithms thus constitute a new contribution to  
655 architectural geometry, connecting statics and geometric design.

656 **Future Work.** There are several directions of future research. One  
657 is to incorporate non-manifold meshes, which occur naturally when  
658 e.g. supporting walls are introduced. It is also obvious that non-ver-  
659 tical loads, e.g. wind load, play a role. There are also some direc-  
660 tions to pursue in improving the algorithms, for instance adaptive  
661 remeshing in problem areas. Probably the interesting connections  
662 between statics and geometry are not yet exhausted, and we would  
663 like to propose the *geometrization* of problems as a general solution  
664 paradigm.

665 **Acknowledgements.** This work was very much inspired by  
666 Philippe Block’s plenary lecture at the 2011 Symposium on Geom-  
667 etry Processing in Lausanne. Several illustrations (the destruc-  
668 tion sequence of Figure 8 and the maximum load example of Figure 9)  
669 have real-world analogues on his web page [Block 2011].

## 670 References

- 671 ANDREU, A., GIL, L., AND ROCA, P. 2007. Computational anal-  
672 ysis of masonry structures with a funicular model. *J. Engrg.  
673 Mechanics* 133, 473–480.
- 674 ASH, P., BOLKER, E., CRAPO, H., AND WHITELEY, W. 1988.  
675 Convex polyhedra, Dirichlet tessellations, and spider webs. In  
676 *Shaping space (Northampton 1984)*. Birkhäuser, Boston, 231–  
677 250.
- 678 BARNES, M. R. 2009. Form finding and analysis of tension struc-  
679 tures by dynamic relaxation. *Int. J. Space Struct.* 14, 2, 89–104.
- 680 BLOCK, P., AND LACHAUER, L. 2011. Closest-fit, compression-  
681 only solutions for free form shells. In *IABSE—IASS 2011 Lon-  
682 don Symposium*, Int. Ass. Shell Spatial Structures. electronic.
- 683 BLOCK, P., AND OCHSENDORF, J. 2007. Thrust network analysis:  
684 A new methodology for three-dimensional equilibrium. *J. Int.  
685 Assoc. Shell and Spatial Structures* 48, 3, 167–173.
- 686 BLOCK, P. 2009. *Thrust Network Analysis: Exploring Three-  
687 dimensional Equilibrium*. PhD thesis, Massachusetts Institute  
688 of Technology.
- 689 BLOCK, P., 2011. Project webpage at [http://block.arch.ethz.ch/  
690 projects/freeform-catalan-thin-tile-vaulting](http://block.arch.ethz.ch/projects/freeform-catalan-thin-tile-vaulting).
- 691 BOBENKO, A., AND SURIS, YU. 2008. *Discrete differential geom-  
692 etry: Integrable Structure*. No. 98 in Graduate Studies in Math.  
693 American Math. Soc.
- 694 BOBENKO, A., POTTMANN, H., AND WALLNER, J. 2010. A  
695 curvature theory for discrete surfaces based on mesh parallelity.  
696 *Math. Annalen* 348, 1–24.
- 697 COHEN-STEINER, D., AND MORVAN, J.-M. 2003. Restricted  
698 Delaunay triangulations and normal cycle. In *Proc. 19th Symp.  
699 Computational Geometry*, ACM, 312–321.
- 700 FRATERNALI, F., ANGELILLO, M., AND FORTUNATO, A. 2002.  
701 A lumped stress method for plane elastic problems and the  
702 discrete-continuum approximation. *Int. J. Solids Struct.* 39,  
703 6211–6240.
- 704 FRATERNALI, F. 2010. A thrust network approach to the equi-  
705 librium problem of unreinforced masonry vaults via polyhedral  
706 stress functions. *Mechanics Res. Comm.* 37, 2, 198 – 204.
- 707 FRIEDLANDER, M. P., 2007. BCLS: Bound constrained least  
708 squares. <http://www.cs.ubc.ca/~mpf/bcls>.
- 709 GIAQUINTA, M., AND GIUSTI, E. 1985. Researches on the equi-  
710 librium of masonry structures. *Archive for Rational Mechanics  
711 and Analysis* 88, 4, 359–392.
- 712 GLYMPH, J., SHELDEN, D., CECCATO, C., MUSSEL, J., AND  
713 SCHOBER, H. 2004. A parametric strategy for free-form glass  
714 structures using quadrilateral planar facets. *Automation in Con-  
715 struction* 13, 2, 187 – 202.
- 716 HEYMAN, J. 1966. The stone skeleton. *Int. J. Solids Structures* 2,  
717 249–279.
- 718 HEYMAN, J. 1995. *The Stone Skeleton: Structural Engineering of  
719 Masonry Architecture*. Cambridge University Press.
- 720 HEYMAN, J. 1998. *Structural Analysis: A Historical Approach*.  
721 Cambridge University Press.
- 722 KILIAN, A., AND OCHSENDORF, J. 2005. Particle-spring sys-  
723 tems for structural form finding. *J. Int. Assoc. Shell and Spatial  
724 Structures* 46, 77–84.
- 725 LIPMAN, Y., SORKINE, O., COHEN-OR, D., LEVIN, D., ROSSI,  
726 C., AND SEIDEL, H. 2004. Differential coordinates for interac-  
727 tive mesh editing. In *Proc. SMI*. IEEE, 181–190.
- 728 LIU, Y., POTTMANN, H., WALLNER, J., YANG, Y.-L., AND  
729 WANG, W. 2006. Geometric modeling with conical meshes  
730 and developable surfaces. *ACM Trans. Graphics* 25, 3, 681–689.  
731 Proc. SIGGRAPH.
- 732 LIVESLEY, R. K. 1992. A computational model for the limit anal-  
733 ysis of three-dimensional masonry structures. *Meccanica* 27,  
734 161–172.

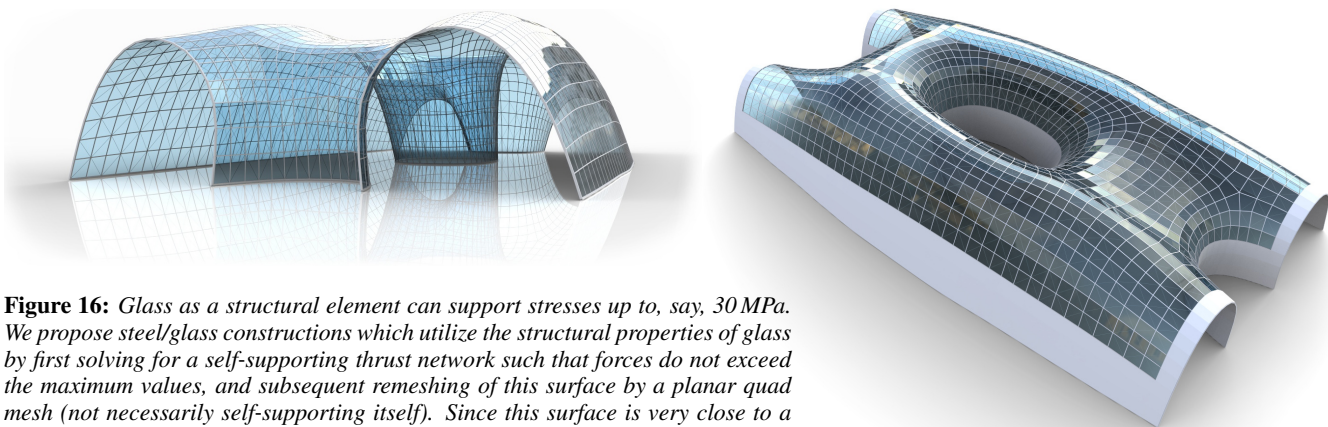


**Figure 16:** Glass as a structural element can support stresses up to, say, 30 MPa. We propose steel/glass constructions which utilize the structural properties of glass by first solving for a self-supporting thrust network such that forces do not exceed the maximum values, and subsequent remeshing of this surface by a planar quad mesh (not necessarily self-supporting itself). Since this surface is very close to a self-supporting shape, joints will experience low bending and torsion moments.

735 MAXWELL, J. 1864. On reciprocal diagrams and diagrams of  
736 forces. *Philosophical Magazine* 4, 27, 250–261.

737 O'Dwyer, D. 1998. Funicular analysis of masonry vaults. *Computers and Structures* 73, 187–197.

739 PAIGE, C. C., AND SAUNDERS, M. A. 1975. Solution of sparse  
740 indefinite systems of linear equations. *SIAM J. Num. Analysis*  
741 12, 617–629.

742 POTTMANN, H., AND LIU, Y. 2007. Discrete surfaces in isotropic  
743 geometry. In *Mathematics of Surfaces XII*, M. Sabin and J. Winkler,  
744 Eds., vol. 4647 of *LNCS*. Springer, 341–363.

745 POTTMANN, H., LIU, Y., WALLNER, J., BOBENKO, A., AND  
746 WANG, W. 2007. Geometry of multi-layer freeform structures  
747 for architecture. *ACM Trans. Graphics* 26, 3, #65,1–11. Proc.  
748 SIGGRAPH.

749 SCHIFTNER, A., AND BALZER, J. 2010. Statics-sensitive layout  
750 of planar quadrilateral meshes. In *Advances in Architectural Ge-  
751 ometry 2010*, C. Ceccato et al., Eds. Springer, Vienna, 221–236.

752 SCHIFTNER, A. 2007. *Planar quad meshes from relative principal  
753 curvature lines*. Master's thesis, TU Wien.

754 SORKINE, O., COHEN-OR, D., AND TOLEDO, S. 2003. High-  
755 pass quantization for mesh encoding. In *Symposium Geometry  
756 processing*, L. Kobbelt, P. Schröder, and H. Hoppe, Eds. Euro-  
757 graphics Assoc., 42–51.

758 VAN MELE, T., AND BLOCK, P. 2011. A novel form finding  
759 method for fabric formwork for concrete shells. *J. Int. Assoc.  
760 Shell and Spatial Structures* 52, 217–224.

761 WÄCHTER, A., AND BIEGLER, L. T. 2006. On the implemen-  
762 tation of a primal-dual interior point filter line search algorithm for  
763 large-scale nonlinear programming. *Math. Progr.* 106, 25–57.

764 WARDETZKY, M., MATHUR, S., KÄLBERER, F., AND GRIN-  
765 SPUN, E. 2007. Discrete Laplace operators: No free lunch.  
766 In *Symposium on Geometry Processing*, A. Belyaev and M. Gar-  
767 land, Eds. Eurographics Assoc., 33–37.

768 WHITING, E., OCHSENDORF, J., AND DURAND, F. 2009. Proce-  
769 dural modeling of structurally-sound masonry buildings. *ACM  
770 Trans. Graphics* 28, 5, #112,1–9. Proc. SIGGRAPH Asia.